Hierarchical macroscopic fibrillar adhesives: In-situ study of buckling and adhesion mechanisms on wavy substrates

Christina T. Bauer[1,3], Elmar Kroner[1], Norman A. Fleck[2], Eduard Arzt[1,3]

[1]INM – Leibniz Institute for New Materials, Campus D2 2, 66123 Saarbrücken, Germany

[2]University of Cambridge, Engineering Department, Trumpington Street, Cambridge, CB2 1PZ, UK

[3]Saarland University, Campus D2 2, 66123 Saarbrücken, Germany

E-mail: eduard.arzt@leibniz-inm.de

Abstract

Nature uses hierarchical fibrillar structures to mediate temporary adhesion to arbitrary substrates. Such structures provide high compliance such that the flat fibril tips can be better positioned with respect to asperities of a wavy rough substrate. We investigated the buckling and adhesion of hierarchically structured adhesives in contact with flat smooth, flat rough and wavy rough substrates. A macroscopic model for the structural adhesive was fabricated by molding polydimethylsiloxane into pillars of diameter in the range 0.3 mm to 4.8 mm, with up to three different hierarchy levels. Both flat-ended and mushroom-shaped hierarchical samples buckled at preloads one quarter that of the single level structures. We explain this behaviour by a change in the buckling mode; buckling leads to a loss of contact and diminishes adhesion. Our results indicate that hierarchical structures can have a strong influence on the degree of adhesion on both flat and wavy substrates. Strategies are discussed that achieve highly compliant substrates which adhere to rough substrates.

Keywords: adhesion, buckling, bioinspired, gecko, hierarchy, PDMS, pillar

1. Introduction

Animals such as various species of insects, spiders and lizards, can adhere to different kinds of substrates [1-6]. They have developed hairy attachment systems which enable them to stick to a wide range of substrate roughness. The gecko, for this purpose, possesses a hairy dry adhesion system with at least three levels of hierarchy [7-10]: the toe pad substrate consists of lamellae covered with setae, which branch into even finer spatulae. It has been suggested that geckos have adapted to generate much higher adhesive forces than is strictly necessary for flat smooth substrates: this redundancy in adhesion allows them to adhere to rough substrates [11-14].

Adhesion of patterned structures to rough substrates has received comparatively little attention in the literature to date. Several research groups have developed artificial gecko-inspired adhesion substrates [15-24] or even hierarchical structures [25-34], but only few studies exist on bioinspired adhesion structures on rough substrates [35-38]; some papers address adhesion of an artificial hierarchical system to rough substrates [39-45] and experiments with living geckos on engineered rough substrates has been made [46]. Furthermore simulation of artificial gecko array on rough surfaces has been conducted [47]. Several theoretical studies suggest that the introduction of structural hierarchy increases adhesion to rough substrates [48-50], but experimental evidence is lacking.

The aim of the present study is to explore the role of structural hierarchy on adhesion to a micro- and macrorough substrate. We report experiments on hierarchically structured model adhesives, with millimeter-size "macroscopic" pillars on flat and wavy substrates. A macroscopic model allows the contact and deformation phenomena of the system to be observed [51-52], thereby giving detailed insight into the interaction mechanisms. The results suggest that a hierarchical structuring of dry adhesives does not necessarily result in increased adhesion. Rather, a new design path for artificial fibrillar adhesives on rough substrates can be derived.

2. Materials and methods

Adhesion experiments were performed on samples with different levels of structural hierarchy, i.e. one, two, and three levels of hierarchy. Further, the tips of the structures were modified to resemble two different geometries, i.e. flat tips and mushroom shaped tips. The samples were brought in contact with flat smooth, flat rough and wavy rough substrates in order to explore the sensitivity of adhesion to substrate topography and structural hierarchy.

Polydimethylsiloxane (PDMS, Sylgard 184 kit, Dow Corning MI, USA) was chosen for its properties in replication precision and handling. At the low testing velocities, PDMS is believed to have low viscoelasticity at room temperature; it is recognized that the presence of viscoelasticity strongly influences adhesion and would thereby complicate the interpretations of our experiments [53-54].

2.1 Preparation of hierarchical macroscopic pillars

Hierarchical structures were made from self-similar cylindrical pillars, as shown in figure 1. At each level of hierarchy, a set of 7 pillars was arranged in a hexagonal pattern with a central pillar, see figure 1(c). Each set was bonded to the top of a larger pillar at the next hierarchy level. This pattern was repeated on moving up the scale of dimension, such that there are 3 levels of hierarchy, with a linear scale factor of ca. 4 on moving from one size to the next. The smallest pillars, 'size 1', are of diameter $D = 0.3$ mm, the intermediate pillars, 'size 2', are of diameter 1.3 mm and the largest pillars, 'size 3', are of diameter 4.8 mm. The center-to-center spacing S of each pillar equals twice the pillar diameter. H is the height of the pillars, L the length of the backing layer, and B is the thickness of the backing layer.

Table 1 summarizes the dimensions of the pillars in terms of the parameters, as defined in figure 1, and presents the magnitude of the second moment of area I and Young's Moduli E, which were measured by beam deflection of each pillar under a transverse load. Samples were prepared with one hierarchy level (HL1), consisting of only size 1 pillars, two hierarchy levels (HL2) with size 1 and size 2 pillars, and three hierarchy levels (HL3) with size 1, size 2 and size 3 pillars. Figure 1 shows a HL3 sample as schematic (figure 1(a)) and as photograph (figure 1(b)).

Table 1: Geometric parameters of the structures for different hierarchy sizes.

parameter	size 1	size 2	size 3
H_i (mm)	1.2	4.9	19.5
D_i (mm)	0.3	1.2	4.8
L_i (mm)	2.1	8.4	33.6
B_i (mm)	≈ 0.8	≈ 2.5	≈ 7.0
S_i (mm)	0.6	2.4	9.6
I_i (m^4)	$4.0*10^{-16}$	$1.0*10^{-13}$	$2.6*10^{-11}$
E_i (MPa)	2.4	3.0	2.6

Samples were cast in PDMS using aluminum alloy molds, as reported previously [51,55]. The PDMS material was prepared by mixing the pre-polymer and cross-linker in a 10:1 ratio. To remove air bubbles, the mixture was degassed in a desiccator. After pouring into the casting molds, the PDMS was fully cured in an oven for more than 12 hours at 75°C. Subsequently, the PDMS pillar structure was peeled from the mold and excess material was removed with a scalpel. The pillars of different size were bonded by a droplet of uncured PDMS, followed by a thermal cure. The above process steps produced PDMS samples with a Young's modulus E = 2.4 to 3.0 MPa as measured by tensile tests. Single pillar size 1 structures were fabricated in the same manner as described before but after the demolding process the pillars around the middle pillar were cut so that only one pillar remained.
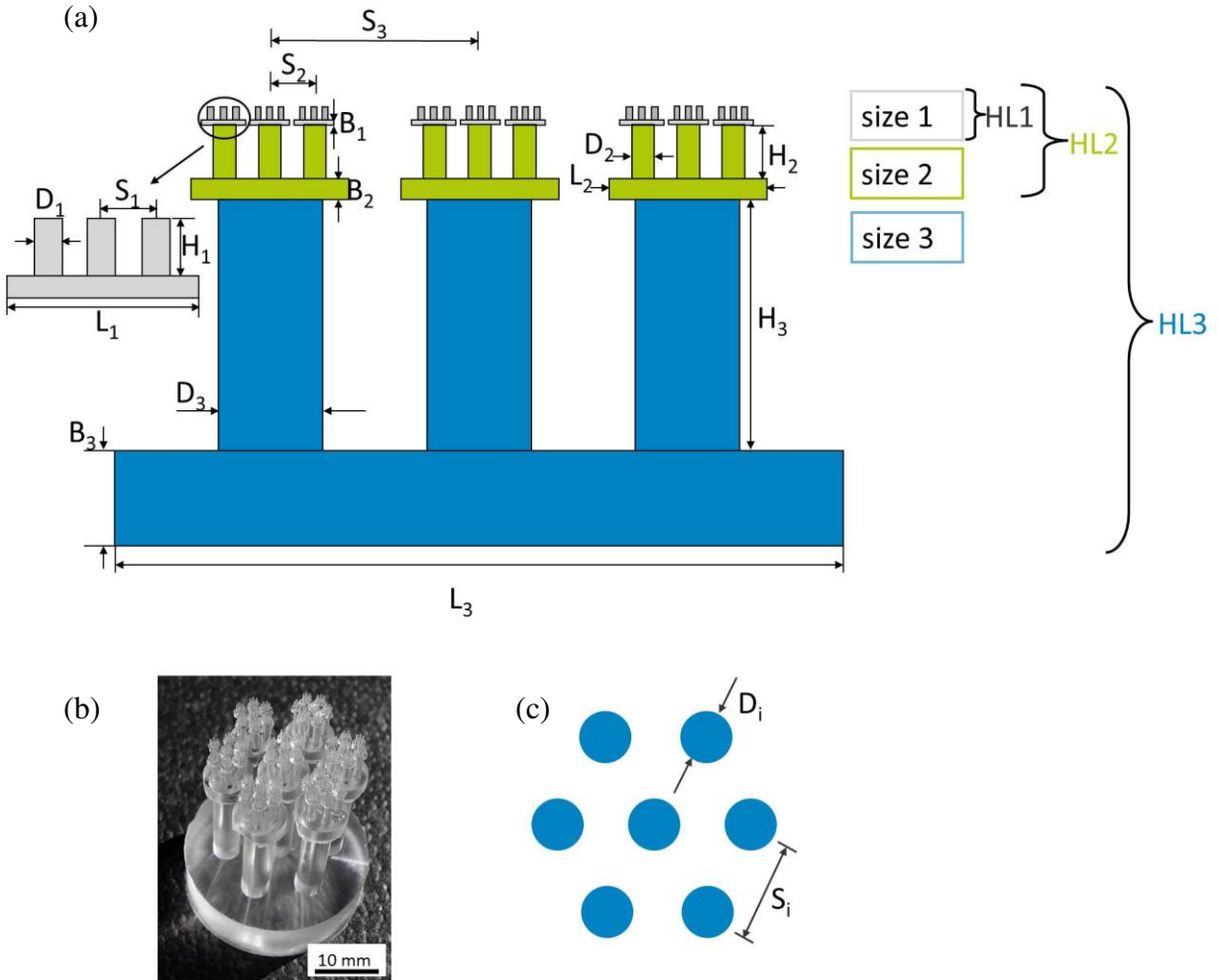
Figure 1: Hierarchical array of the macroscopic pillars. (a) Schematic overview of the hierarchical array; (b) photograph of a sample with three hierarchical levels (HL3); (c) end view of hexagonal arrangement of 7 pillars at each level of hierarchy.

2.2 Preparation of mushroom tips on size 1 pillars

In all adhesion experiments the contact elements were the tips of the size 1 pillars, in either the as-cast flat end geometry or in a so-called 'mushroom' geometry. To achieve the mushroom geometry, the tips of size 1 pillars were modified using the following steps as previously established [20].

(i)   A droplet of liquid PDMS was deposited onto each size 1 pillar by dipping the set of 7 pillars into a thin layer of uncured PDMS.

5

(ii)   The droplets were deformed into a mushroom shape by pressing the pillars against a glass slide for a period of 12 hours at 75°C. The glass slides were pre-treated by placing a 50/50 mixture of perfluorodecyltriethoxysilane and hexane adjacent to the glass slides in a desiccator, until complete evaporation occurred under vacuum. The glass plates were maintained at 95°C for 30 minutes to stabilize the silanized surface. This allowed for easy removal of the cured PDMS from the glass.

(iii)   After cure, the pillars were peeled from the glass slides.

Figure 2 shows a schematic of a mushroom shaped tip. The geometry of the tips was determined by optical microscopy and the following sizes, as described in figure 2, were found: height $H \approx 75$ µm, width $W \approx 40$ µm, angle $\alpha \approx 50°$ and tip radius $\rho \approx 20$ µm.
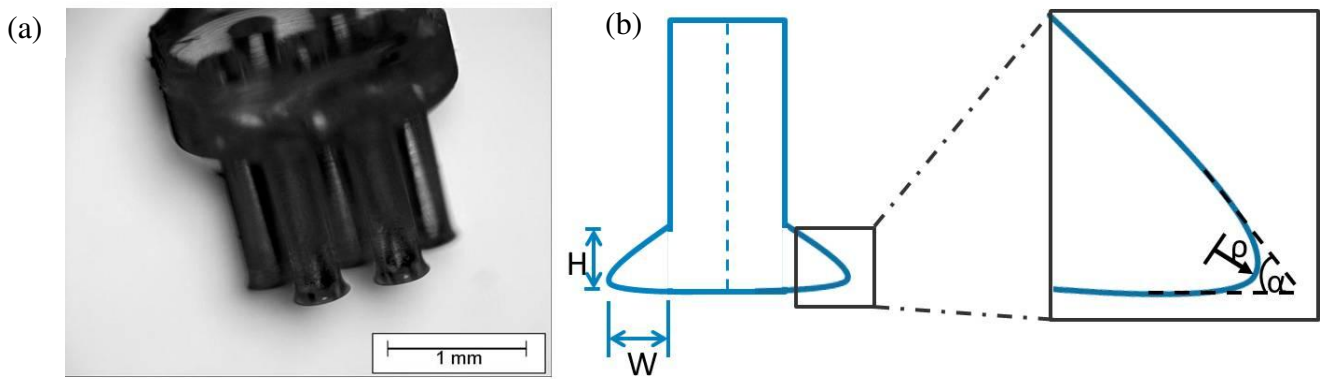

Figure 2: (a) Optical micrograph of mushroom shaped tips of size 1 pillars after the dipping process, (b) schematic of a mushroom shaped tip with the geometry parameters height H, width W, the angle α of the mushroom cap and tip radius ρ (not drawn to scale).

2.4 Adhesion and buckling measurements

Adhesion measurements were performed on a test apparatus, called Macroscopic Adhesion measurement Device (MAD) [56]. The samples were fixed on a glass slide and placed on a positioning stage. A flat substrate of borosilicate glass and two aluminum substrates with wavy surfaces were used as substrate

surfaces. The machined aluminum substrates had a surface finish of 0.4-0.5 µm (root-mean-square) and 200-250 µm (RSm). In contrast the borosilicate glass substrate had a surface finish of 0.01 µm (root-mean-square) and 10 µm (RSm). The roughness was measured by a profilometer. The wavy rough substrates had the following surface topography:

- sinusoidal: wavelength of 4 mm and a peak-peak height of 200 µm, see figure 3a and b.

- truncated sinusoidal: wavelength of 2 mm and a peak-peak height of 200 µm, but with flattened tops of width 1 mm, see figure 3c and d.

The waviness of the substrates represents macroroughness. Force sensing was realized by a combination of a spring and a laser interferometer. A mirror was attached to the spring, which reflected the laser beam, thus allowing the determination of the spring deflection. The spring constant was determined by calibration with a load cell, and was found to be 2525 N/m. For all measurements a video of the sample deformation was recorded in side view.
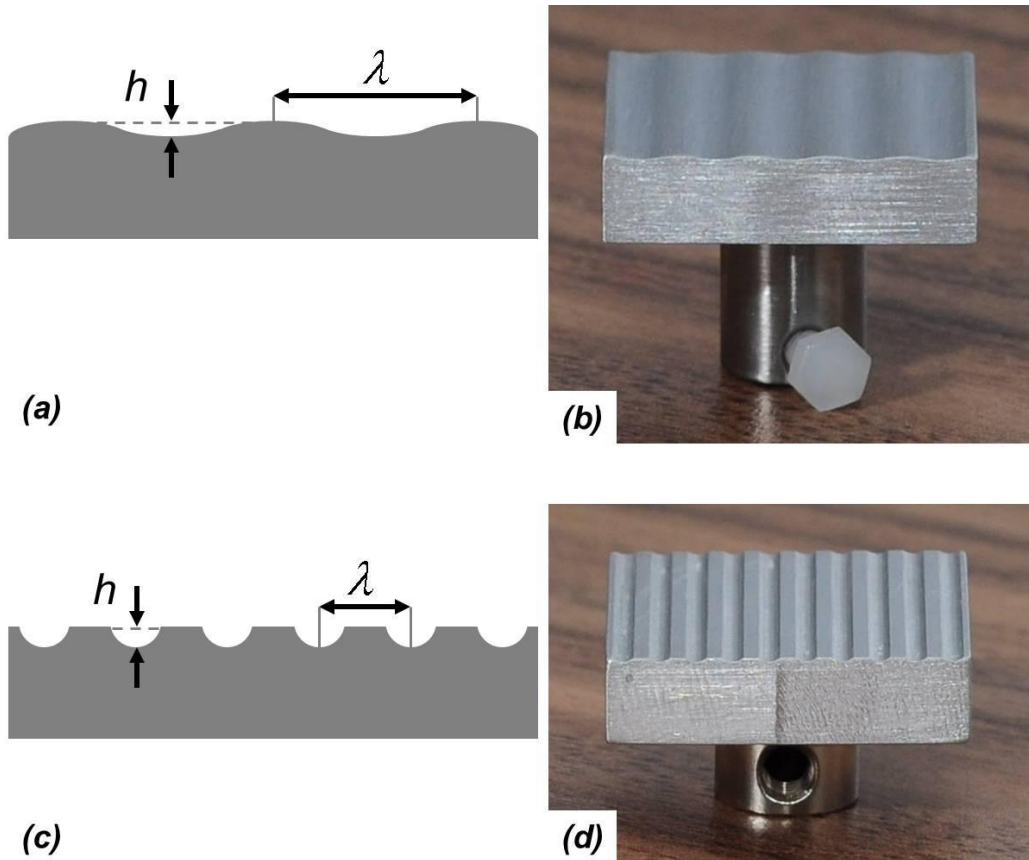
Figure 3: Substrate surfaces with wavy contours for adhesion testing. (a) Schematic and (b) photograph of the sinusoidal aluminum substrate (λ = 4 mm, h = 200 µm), (c) schematic and (d) photograph of the truncated sinusoidal aluminum substrate (λ = 2 mm, h = 200 µm).

In addition to adhesion, the compressive buckling preload was measured. It was found that adhesion was limited by the onset of buckling under the pre-load. Adhesion and buckling measurements were performed on all level combinations (HL1, HL2 and HL3), with and without mushroom shaped tips. The measurements were performed by moving the sample towards the substrate, applying a predefined preload P, and retracting again until pull-off occurred. The measurements with the flat sample were carried out using glass and aluminum substrates and were repeated three times for each substrate. To determine the pull-off force, F, 15 measurements were performed for each measurement set. Adhesion measurements on the flat rough substrate were performed on the flat part of the truncated sinusoidal aluminum substrate with single pillars to ensure that the probes had the same microroughness. The results from single pillar

8

measurements were multiplied by 7 for comparison with the other measurements. Adhesion measurements on the two wavy rough substrates were performed at different positions with respect to the wavelength of roughness. This was achieved by changing the position along the wavelength in 0.2 mm steps. Scanning one wavelength of the wavy substrate resulted in 21 measurements for the sinusoidal substrate, and 11 measurements for the truncated sinusoidal substrate for each scan. Prior to all measurements, repeated contacts ensured that the substrate had a stable configuration [57] and was well aligned [58]. The correct alignment was checked with an optical camera setup. In all tests of type HL1, HL2 and HL3, the substrate surface was in contact with a single set of 7 pillars of size 1, and the measured force is the total force on all 7 pillars (with the exception of additional single pillar measurements as detailed below). For tests on HL2, the loaded set of 7 pillars of size 1 was placed on a central pillar of size 2. For tests on HL3, the loaded set of 7 pillars of size 1 was placed on the central pillar of a hexagonal arrangement of 7 pillars of size 2 and in turn the 7 pillars of size 2 were bonded to a central pillar of size 3. The error bars in all graphs represent the standard deviation about the arithmetic mean value.

3. Results

3.1 Adhesion experiments using a flat substrate

Representative force-displacement curves for the total force on 7 pillars of a HL1 sample with mushroom shaped tips are given in figure 4a. The peak positive force is defined as compressive preload P, whereas the peak negative force is defined as the pull-off force F, as shown in figure 4(a). When the preload is sufficiently high, buckling occurs at $P = P_B$, as shown in the rightmost plot of figure 4(a). The dependence of F upon P is given in figure 4(b); three regimes can be identified. Representative plots of force versus displacement for each regime are shown in figure 4(a), and each regime is now described in turn.

Regime I ($P \ll P_B$): For 0 mN < P < 30 mN F increases steeply with increasing P due to contact formation. A low preload $P \approx 30$ mN is required to form contact between all pillar tips and the substrate. A force-displacement curve in this regime shows a small compressive (preload P) and a low tensile value (pull-off force F).

Regime II ($P < P_B$): F increases slightly with increasing P for 30 mN $< P <$ 330 mN. This is ascribed to the fact that microscopic asperities on the contacting tip are flattened by increasing P. A force-displacement curve in this regime shows higher compression and higher tension compared to Regime I.

Regime III ($P = P_B$): The pillars buckle elastically at a critical preload $P_B \approx 340$ mN. Then the preload P saturates at $P = P_B$ and the pull-off force F decreases with increasing displacement in the post-buckling regime. The peak pull-off force F_{max} occurs at the onset of elastic buckling at $P = P_B$, as shown in figure 4b.
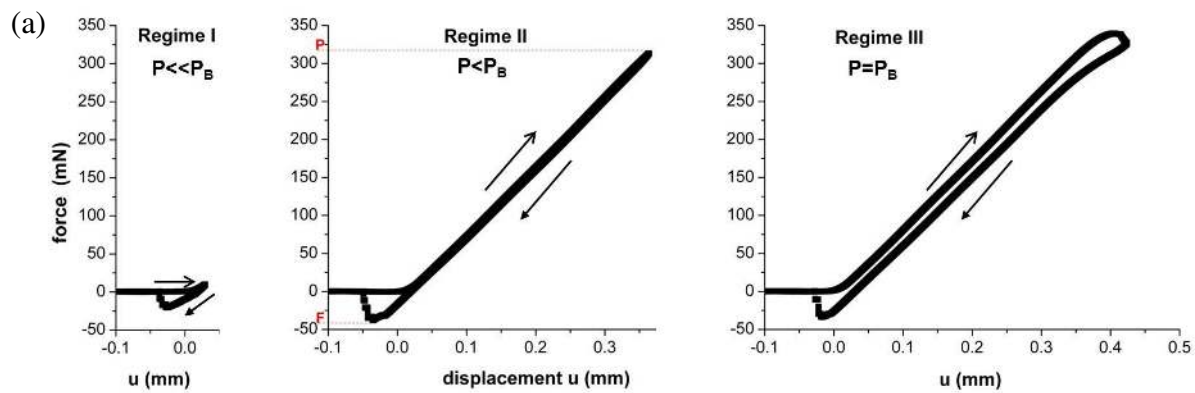
(a)

(b)

10
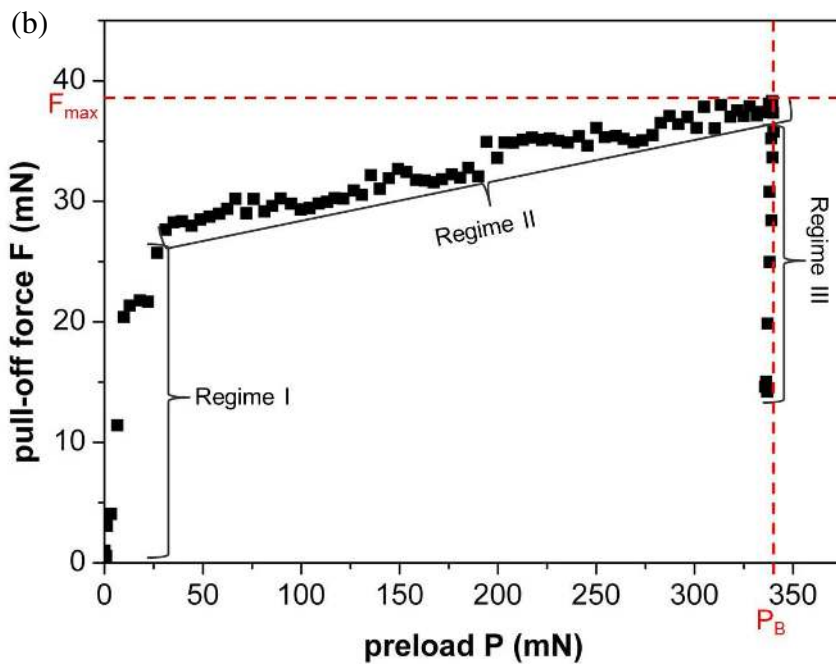
Figure 4: (a) Force-displacement curves of three different characteristic regimes for an HL1 sample with mushroom shaped tips on the flat glass substrate, measured on all 7 pillars. The sample approaches the substrate and forms contact (Regime I); with higher displacement the pull-off force F increases (Regime II) until a critical preload P is reached (Regime III). The pull-off force F decreases with increasing displacement. The peak load is determined as the buckling preload P_B. (b) The pull-off force F as a function of preload P is given for an HL1 sample with mushroom shaped tips on the flat glass substrate, measured on all 7 pillars. The pull-off force F increases with increasing preload, until a critical preload P_B is reached. Above the critical preload P_B, further sample compression does not lead to an increase in preload P but to a collapse of the structures and subsequently to a drop in pull-off force F.

Representative snapshots of the buckling mode for HL1, HL2 and HL3 sample are shown in figures 5a, b, and c, respectively. In the case of HL2 and HL3, the pillars of size 2 and 3 buckled in the opposite direction to that of the pillars of size 1.
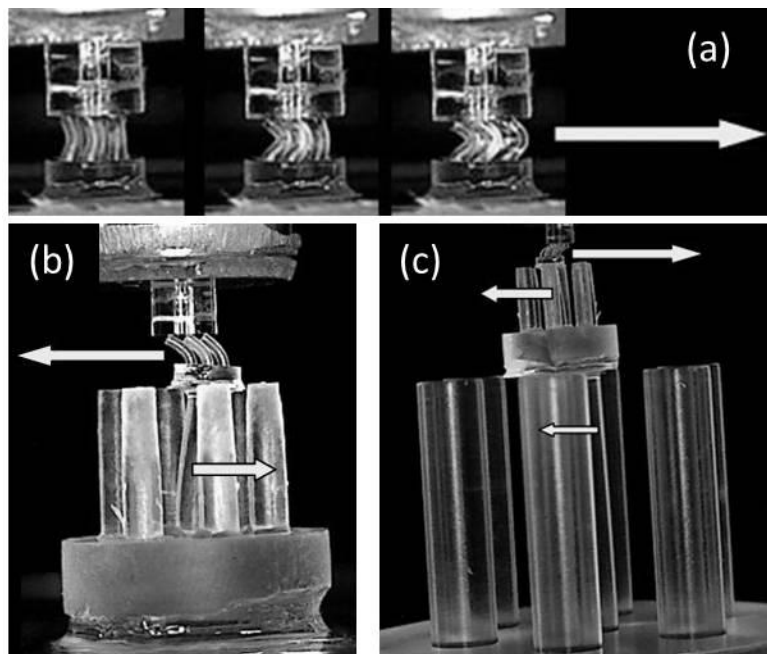

Figure 5: Buckling mode as a function of hierarchy level for (a) HL1, (b) HL2 and (c) HL3, measured against a flat substrate. The arrows indicate the direction in which the pillars deflect.

The buckling preload P_B for the three levels of hierarchy and for the two types of tip shapes against a flat substrate is shown in figure 6a. Note that the buckling preload P_B of a single hierarchy level HL1 is about 4 times that for hierarchy levels HL2 and HL3. The buckling preload P_B has comparable values for both flat and mushroom tip structures: the presence of the mushroom tip has a negligible effect upon the value of P, and upon the buckling mode.
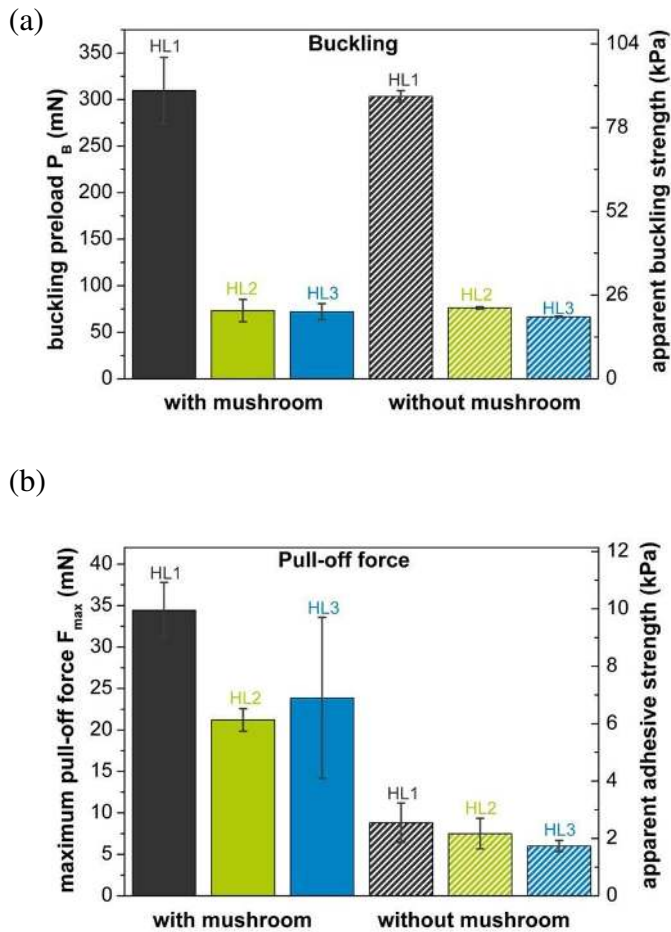
(a)

(b)

Figure 6: Critical preload P_B and pull-off forces F_{max}, as well as the corresponding 'apparent' strength values, measured on all 7 pillars of size 1: (a) Buckling preloads P_B for different specimens measured against the flat glass substrate: HL1, HL2 and HL3 structures, with and without mushrooms. (b) Pull-off force F_{max} for HL1, HL2 and HL3 structures with and without mushrooms measured against the same substrate.

Figure 6b shows the maximum pull-off forces F_{max} upon reaching the critical buckling preload. Here, the single-level structure HL1 displays a slightly higher pull-off force F_{max} than the hierarchical structures HL2 and HL3. The mushroom shaped tip structures showed an enhancement in pull-off force F_{max} by up to a factor of 3 to 30 compared to the flat tips.

The corresponding adhesive strength ("apparent" and "actual") values are presented in table 2. For the calculations of the "apparent" adhesive strength, the apparent contact area was chosen as $(L_1^2 \pi/4) = 3.46$ mm² (see also figure 1 and table 1). For the calculations of the "actual" adhesive strength, the contact area was chosen for structures without mushroom as $7(D_1^2 \pi/4) = 0.49$ mm² and for structures with mushroom as $7((D_1+2W)^2 \pi/4)$ (see also figure 1, table 1 and figure 2).

Table 2: Adhesive strength values of HL1, HL2 and HL3 structures with and without mushrooms measured against a flat glass substrate.

structure	"apparent" adhesive strength (kPa)	"actual" adhesive strength (kPa)
HL1/m	9.94 ± 0.97	43.58 ± 4.25
HL2/m	6.12 ± 0.39	26.84 ± 1.72
HL3/m	6.89 ± 2.80	30.20 ± 12.29
HL1	2.54 ± 0.68	17.97 ± 4.84
HL2	2.17 ± 0.53	15.30 ± 3.75
HL3	0.23 ± 0.31	12.25 ± 1.36

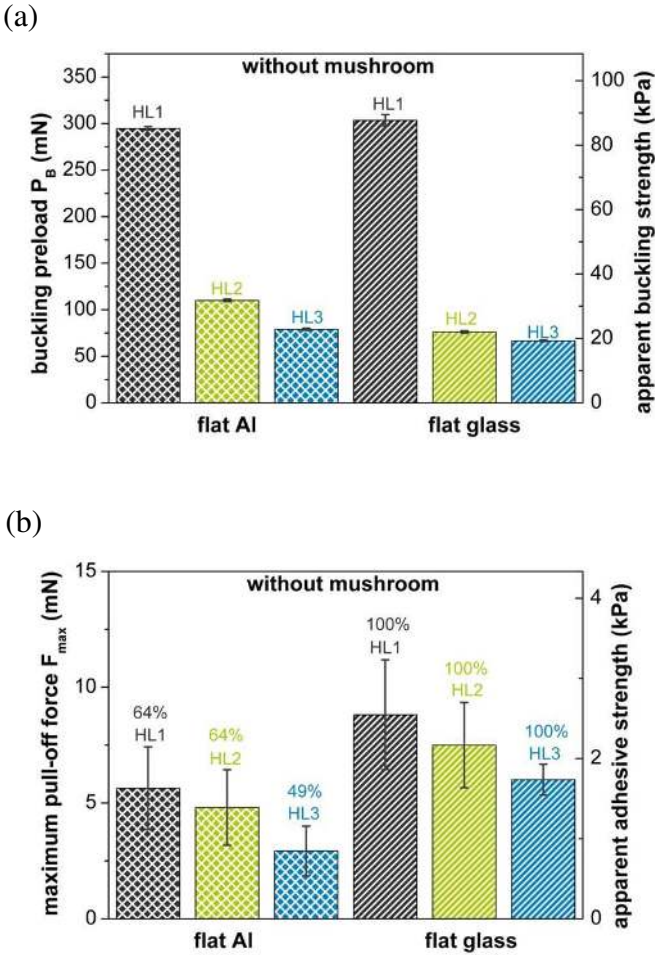*3.2 Adhesion experiments using a flat rough substrate*

(a)

(b)

Figure 7: (a) Critical preload P_B and (b) pull-off forces F_{max}, , as well as the corresponding 'apparent' strength values: Measurements on single pillar on flat aluminum and on all 7 pillars of size 1 on flat glass: HL1, HL2 and HL3 structures without mushrooms. The results from single pillar measurements were multiplied by 7 for comparison with the other measurements.

The buckling preload P_B for the three levels of hierarchy against a flat rough aluminum substrate and flat smooth glass substrate is shown in figure 7(a). The buckling preload of a single hierarchy level HL1 is again about 4 times higher than for hierarchy levels HL2 and HL3. It is seen that the presence of microroughness has negligible effect on the buckling mode.

14

Figure 7(b) shows the maximum pull-off forces F_{max} upon reaching the critical buckling preload. Here, the single-level structure HL1 displays a higher pull-off force F_{max} than the hierarchical structures HL2 and HL3. HL3 shows the lowest pull-off force F_{max}. The microroughness of the flat rough aluminum substrate showed a decrease in pull-off force F_{max} by up to 35 to 50% compared to the flat smooth glass substrate.

3.3 Adhesion experiments using a wavy rough substrate

The hierarchical pillars were pressed against the sinusoidal substrate of wavelength $\lambda = 4$ mm until a buckling event (at least buckling of one HL1 pillar) occurred. Figure 8(a) shows the buckling load P_B for 7 pillars as a function of testing position y, as defined in figure 8(b). The schematic below the graph depicts the position of the contacting elements with respect to the wavy substrate; the dots indicate the center position of the center pillar of the hexagonal array. Figure 8(b) also shows the maximum pull-off force F_{max}.
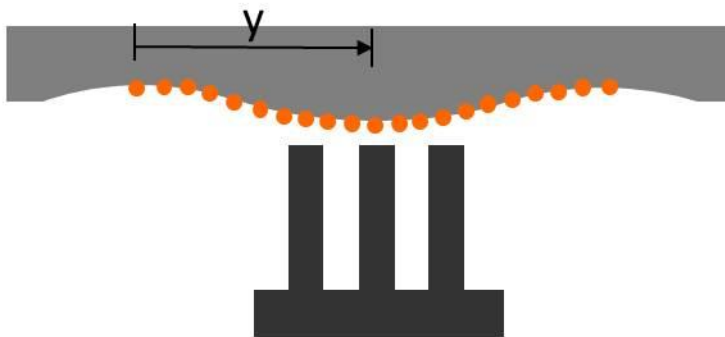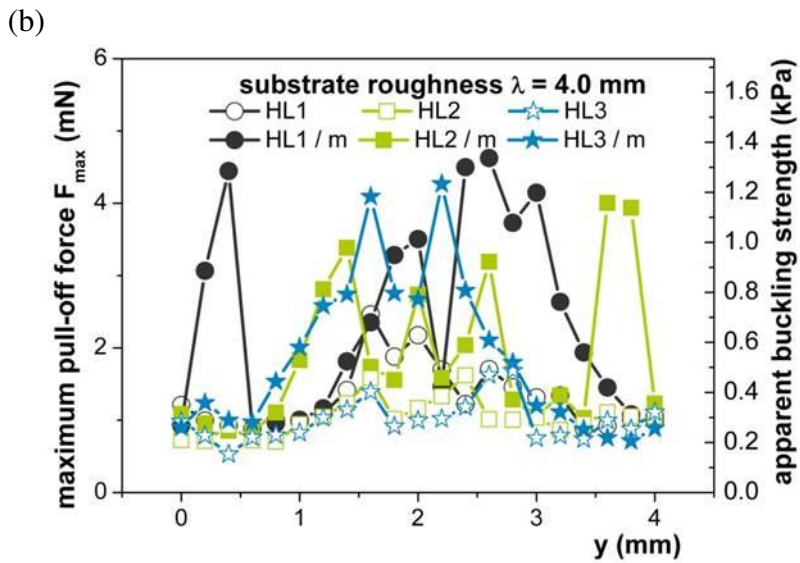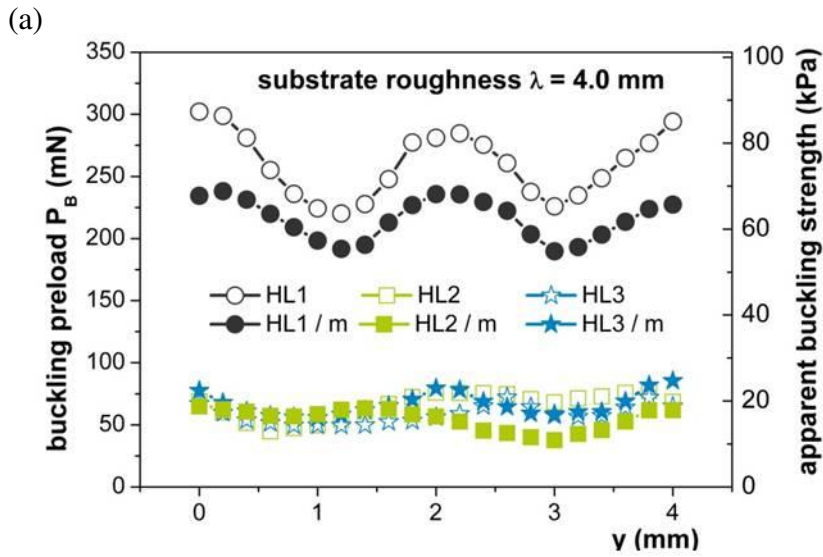
(a)

(b)

Figure 8: Measurement results on samples with HL1, HL2 and HL3, both with flat tips and mushroom tips (indicated as "/ m") measured on all 7 pillars of size 1. The forces were measured with a wavy substrate (λ
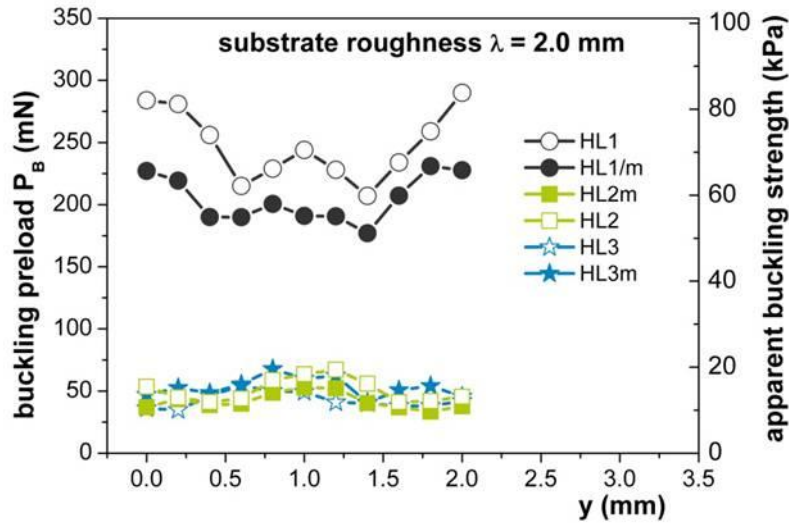
= 4 mm, h = 200 µm) as a function of substrate position. a) Buckling preload P_B and b) maximum pull-off force F_{max} , with the corresponding 'apparent' strength values. The schematic below shows the testing position of the center pillar with respect to the wavy substrate (drawn with correct relative scale).

The buckling preload values P_B differ significantly for the HL1, HL2 and HL3 samples, recall figure 8(a). Generally, the single-level structure HL1 exhibits the highest buckling loads, but there is also a large variation with position; these samples buckle at the lowest preload for the substrate positions $\lambda/4$ (y = 1.0 mm) and $3\lambda/4$ (y = 3.0 mm), where the highest slope of the substrate surface is found. Although the shapes of the curves for the HL2 and HL3 samples resemble that of the HL1 sample, the absolute values are lower. Mushroom shaped tips tend to have a slightly decreased buckling preload compared to the flat tip structures.

In similar fashion, the largest values of F_{max} occur at y = 2.0 mm = $\lambda/2$, at the peak of the sine wave. For the HL1, HL2 and HL3 samples, the F_{max} values are comparable, but lower than the adhesion forces obtained by flat substrate measurements. Mushroom-shaped structures always show increased adhesion compared to the flat tip pillars.

Similar experiments were performed with a truncated substrate of wavelength 2 mm. The results are shown in figure 9. Again, a significantly reduced buckling preload P_B is observed for structures with more than one level of hierarchy. The buckling preload curves are also symmetric. The values of F_{max} for the truncated sinusoidal substrate exceed the values in figure 8 for the sinusoidal substrate.
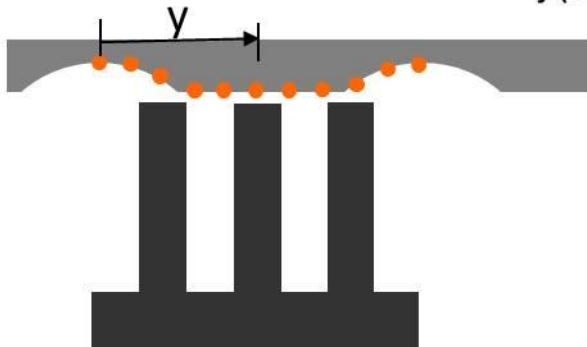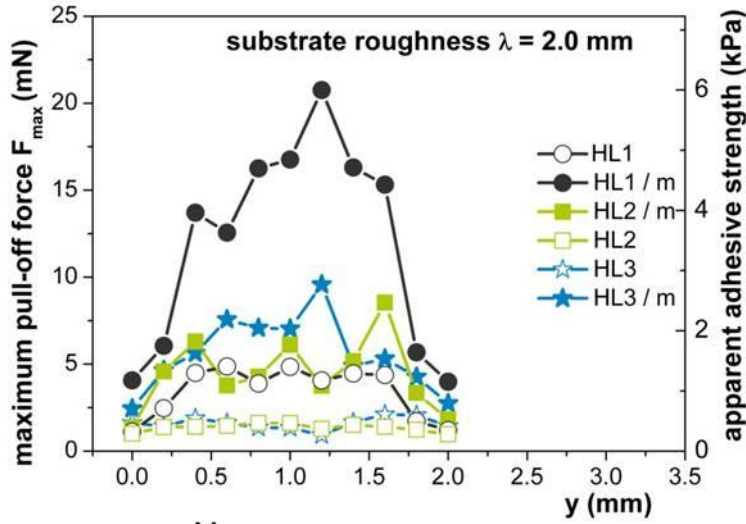
(a)

(b)

Figure 9: Experiments similar to figure 7 but with a truncated sinusoidal substrate. The x-axis shows the position of the sample with respect to the wavy substrate; (a) Buckling force P_B, and (b) maximum pull-off

18

force F_{max}, with the corresponding 'apparent' strength values. Below, a schematic is given showing the wavy substrate and the testing position of size 1 structure.

The buckling preload P_B for the truncated sinusoidal substrate is highest at the positions λ ($y = 0$ mm and $y = 2.0$ mm), i.e. in the valleys of the substrate. Minima in the buckling preload P_B were found at the intermediate positions of the maxima of the substrate, approximately at positions $\lambda/4$ ($y = 0.5$ mm) and $3\lambda/4$ ($y = 1.5$ mm). At positions close to $\lambda/2$ ($y = 1.0$ mm), the substrate is similar to a flat substrate and buckling is delayed to preload values P_B that are about a factor of about 30 to 40% higher than in the lowest buckling positions.

For the maximum pull-off forces F_{max}, shown in figure 8(b), several trends were observed. The HL1 samples adhered better than both the HL2 and HL3 samples, which showed comparable pull-off forces. Again, the substrate symmetry is mirrored in the pull-off forces. The lowest forces were found at positions λ ($y = 0$ mm and $y = 2.0$ mm). The maximum pull-off force F_{max} is almost independent of position for the flat tip HL2 and HL3 structures. Again, mushroom shaped structures showed increased adhesion compared to the flat tip pillars with the same hierarchical structure, independent of the number of hierarchy levels or the testing position. Mushroom tips increased pull-off forces by a factor of 3 to 5. For a better interpretation of the measurements on a wavy substrate, additional measurements with size 1 single pillars will now be reported.

3.4 Size 1 single pillar measurements

In order to gain further insight into adhesion on a wavy substrate, additional single pillar buckling measurements were conducted. Figure 10 shows the measured buckling preload for:

(i) a single pillar ($sp_{experiment}$),

(ii) the theoretical buckling preload for a hexagonal pillar array by making use of single pillar measurement values (hp_{theory}); the definition is given in figure 10.

19

(iii) the measured values for a hexagonal pattern consisting of 7 pillars ($hp_{experiment}$) and

(iv) the measured single pillar values ($s_{p,experiment}$) multiplied by 7 ($7*(sp_{experiment})$).

All values are presented for a sinusoidal punch of wavelength a) $\lambda = 4$ mm, and b) $\lambda = 2$ mm. In figure 10 a the $sp_{experiment}$ values (and the $hp_{experiment}$ results) show lowest values of P_B at $\lambda/4$ ($y = 1.0$ mm) and at $3\lambda/4$ ($y = 3.0$ mm). The measured values for the hierarchically assembled pillars are adequately approximated by multiplying the single pillar value by 7 ($7*(sp_{experiment})$). The procedure was repeated for the truncated sinusoidal substrate ($\lambda = 2$ mm, see figure 10 b)). The $sp_{experiment}$ values show the highest buckling load at the position of the flat part of the substrate as well as at λ ($y = 0$ mm and $y = 2$ mm). Again, the $7*(sp_{experiment})$ values agree reasonably well with the $hp_{experiment}$ values.
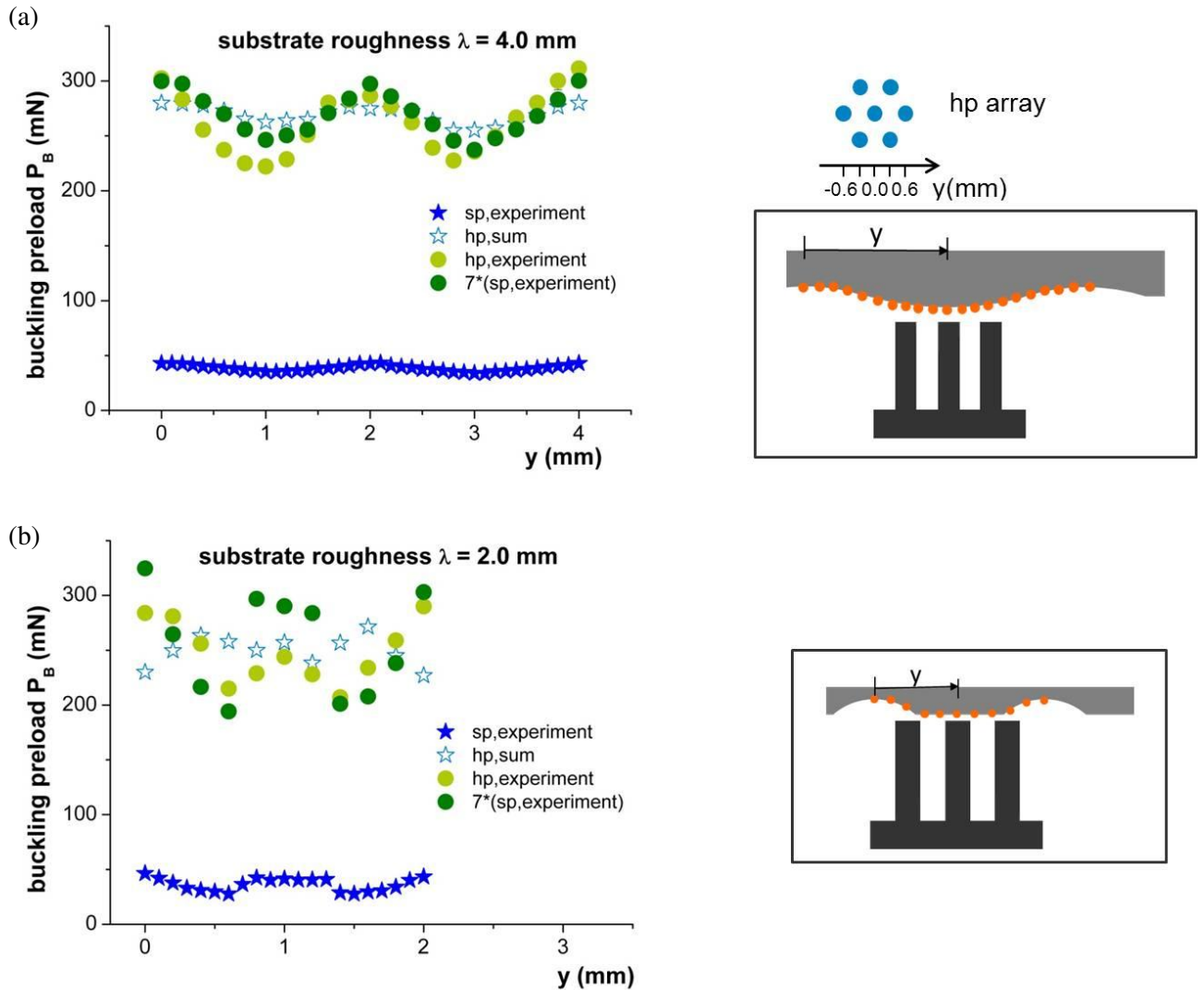
Figure 10: Buckling preloads of a size 1 single pillar (sp) and of a size 1 hexagonal pillar (hp) array: (a) sinusoidal substrate with $\lambda = 4.0$ mm, and (b) truncated sinusoidal substrate with $\lambda = 2.0$ mm. The hp$_{sum}$ values are the sums of the single pillar measurements at the respective positions (see schematic insert).

Figure 11 presents the force - displacement curves of the single pillar (*sp*) at selected positions y on a wavy substrate ($\lambda = 4$ mm) and includes curves for the *hp$_{sum}$* and for the *hp$_{experiment}$* curve. The individual pillars of an HL1 hexagonal pillar array do not make contact simultaneously during the experiment because of the waviness of the substrate. The differences in distance between the substrate and the sample

are measured experimentally and considered in figure 11 by an off-set in the displacement. The respective force-displacement curve exhibits that with increasing displacement the applied preload P on each pillar decreases by 30-40% after the buckling event, then increases again until the sample is retracted from the substrate. The hp_{sum} curve is the sum of the single pillar values for an assumed hexagonal pillar array with consideration of the off-set in the displacement. The hp_{sum} curve and the experimentally measured hp curve show a similar trend, with a buckling load deviation of only 6%.
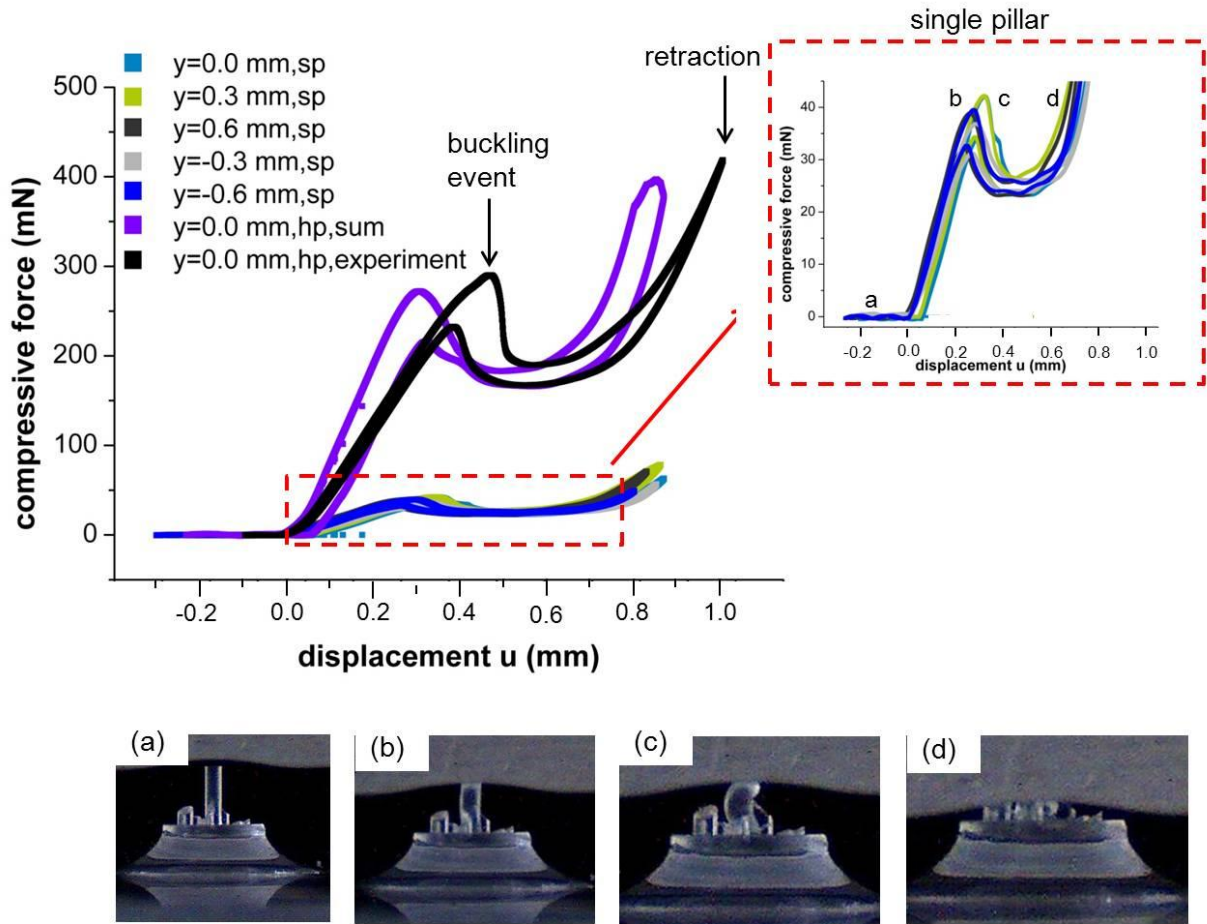

Figure 11: HL1 force/displacement curves measured in compression on a wavy substrate (λ = 4 mm, h = 200 µm): (a) uncompressed, (b) just before buckling, (c) buckled, (d) strongly compressed for the case y = 0.0 mm. The results of the first five measurement curves (y = 0.0, 0.3, 0.6, -0.3, -0.6 mm) are based on size 1 single pillar (sp) measurement results. The "hp$_{sum}$" data points are the sums of the single pillar

measurement at the respective positions. The experimental data curve "hp$_{experiment}$" is based on a real measurement with a hexagonal array of size 1 pillars.

4. Discussion

4.1 Experiments on flat substrates

The experiments on flat substrates have shown that the buckling behaviour of the structures strongly depends on hierarchy. While non-hierarchical (HL1) structures have buckling loads of approx. 300 mN, the hierarchical samples show values of around 75 mN, a factor of 4 lower. This can be explained by the change in the buckling mode with structural hierarchy.

a) Estimation of the buckling load for a single size 1 pillar (H=1.2 mm, D=0.33 mm)

The Euler load P_E for a size 1 pillar is

$$P_E = \pi^2 \frac{EI}{H^2} = 12 \text{ mN}$$

with the assumption of Young's modulus $E = 3$ MPa and second moment of area $I = \frac{\pi}{64} D^4$.

In contrast, a pillar with one end hinged and the other fixed implies a buckling load of 2.04 P_E. Also, the pillar is stocky (aspect ratio = 4), hence Biot [59] finds an elevation in buckling load of 50%. Thus, the predicted buckling load is 3.06 P_E or 37 mN. As the observed buckling load for a single pillar (no mushroom tip) is 43 mN, i.e. 17% above the prediction, the agreement is adequate for our purposes.

b) Estimation of the buckling load for a hierarchical pair of pillars

Now consider the elastic buckling response of a pillar which has a stepwise jump in bending modulus along its length. The predicted ratio of buckling strength for HL1 and HL2 is 2.05/0.423 = 4.8, which again conforms well to the observed ratio of 3.9 to 4.9 (deviation of 2 to 19%). The detailed estimation and derivation is summarized in the Appendices (see Section A1).

The results presented in figure 6b show that there is a notable difference in adhesion (maximum pull-off force) between flat tip structures and structures with mushroom shaped tips, as expected from earlier studies [20,60-61]. For adhesion against flat substrates, the effect of tip shape dominates over the effect of hierarchy. Interestingly, the mushroom shaped structures show buckling load values similar to flat tip structures. This is in contrast to the experiments performed by Paretkar et al. [62-63], who found that mushroom tips can delay buckling. This discrepancy may be ascribed to different mushroom tip geometry, which is more difficult to control in the fabrication process for the microscopic structures.

An important outcome of the present paper is that hierarchical structures tend to show *lower* adhesion compared to single level samples if tested against a flat substrate. A possible explanation is that the hierarchical samples require a higher preload to fully adapt to the substrate, e.g. adaptation to micro- and nanoroughness. However, a high preload cannot be achieved due to buckling, which would lead to a loss in tip contact and thus a loss in adhesion. It can be concluded that the introduction of a hierarchy is not necessarily beneficial: it will not increase adhesion against smooth, flat substrates, but may even reduce it due to the buckling at lower preload for hierarchical structures.

4.2 Experiments on a flat rough substrate

To investigate the influence of microroughness on adhesion, measurements on a flat rough aluminum substrate were made. The adhesion decreased by 35 to 50% in comparison to measurements on a flat smooth glass substrate for HL1, HL2 and HL3. This supports the assumption that microroughness decreases adhesion [64]. Fuller and Tabor [64] correlated the decrease of adhesion with an 'adhesion parameter' $1/\Delta c$

$$\frac{1}{\Delta c} = \left(\frac{4\sigma}{3}\right)\left[\frac{4E}{3\pi\beta^{\frac{1}{2}}\Delta\gamma}\right]^{\frac{2}{3}}$$

where σ is the root-mean-square roughness, E the Young's modulus, β the radius of curvature of asperity and ΔΥ the surface energy (0.02 J/m^2). The radius of curvature of asperity β of the substrate can be calculated as

$$\beta = \frac{\chi^2}{4\pi^2\sigma}$$

where χ is the RSm roughness of the substrate, i. e. the average groove spacing of the roughness. In figure 12 the relative pull-off force is plotted as a function of the adhesion parameter. The adhesion parameters for flat smooth glass and flat rough aluminum substrate were calculated: $1/\Delta c_{glass}$ = 0.029 and $1/\Delta c_{Al}$ = 0.656. This means that for the flat glass substrate no relevant adhesion decrease is expected in contrast to the rough aluminum substrate, for which a decrease of about 32% is predicted. Our result of 35% for HL1 and HL2 is in good agreement with this value.
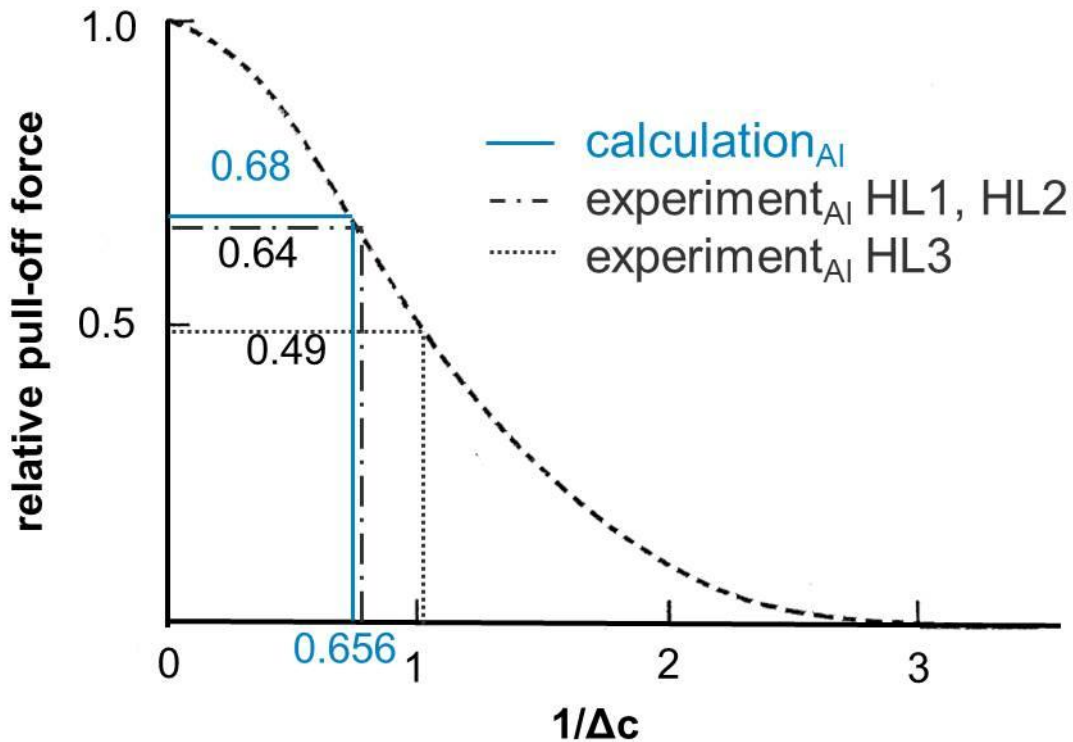
Figure 12: Relative pull-off force plotted as a function of the adhesion parameter $1/\Delta c$, modified after Fuller and Tabor [64], with calculated relative pull-off force and experimental values of HL1, HL2 and HL3 on flat rough aluminum.

4.3 Experiments on wavy rough substrates

In our study, we used two different wavy rough substrate surfaces to test the adhesive behaviour of fibrillar substrates. Some generic observations were made that shed light on buckling and adhesion mechanism. In the experiments on wavy rough substrates, mushroom shaped structures adhered better than flat tip structures as expected [20]. The tests on both wavy substrates also showed that the samples adhered best if they were positioned at the peak of the profile, while testing on the substrate surface of maximum inclination gave the lowest adhesion.

The positional dependence of buckling does not differ between the two wavy substrates. For the truncated sinusoidal and the sinusoidal substrate, buckling is favored at the intermediate positions between the wave peaks/flat part and the valleys, leading to a buckling preload with a frequency twice that of the substrate sinus. These findings confirm that the buckling behaviour depends on the surface topography.

The adhesion behaviour differs for the two wavy substrates; for the truncated sinusoidal substrate, the non-hierarchical structures gave the highest pull-off values. Clearly, an introduction of a hierarchy is not favorable here. However, on the sinusoidal wavy substrate, the adhesion – although low – is comparable for the single level and multi-level hierarchical structures. It can be assumed that this is due to the longer wavelength of the substrate protrusions, where the pillars can better adapt to the wavy substrate.

4.4 Size 1 single pillar measurements

The theoretical buckling load value for a size 1 hexagonal pillar array shows that the best agreement was achieved by multiplying the *sp* measurements with the number of pillars and not to add the values according to a theoretical hexagonal pillar array value. But when the off-set of the individual

force/displacement curves (presented in figure 10) is accounted for, the agreement is even better. The repeated increase of the force F with larger displacement after the first buckling process can be explained by contact formation of the lateral side of the pillar. Deviations of hp$_{experiment}$ and hp$_{theory}$ values, which are based on sp measurements, occur because the interactions between the pillars are neglected and cannot be calculated using sp measurements. But the measurements showed that sp measurements can help to achieve a rough prediction for buckling preloads P_B for a hexagonal array on a wavy substrate but cannot replace the measurements with a real hexagonal array.

Overall, the insight created by our mechanistic study suggests that the design of hierarchical fibrillar adhesive surfaces needs to consider both their compressive and adhesive behaviour. It is also likely that different design strategies will have to be applied to different degrees of roughness. The present paper is a first step in the direction of a rational design of such structures.

5. Conclusions

We have carried out a mechanistic study of hierarchical model adhesives in contact with substrate surfaces with model roughness. It can be concluded that the following considerations are essential in the design of hierarchical adhesive structures:

- Irrespective of the number of hierarchies and other parameters, a mushroom tip shape leads to higher adhesion, both for rough and smooth substrates.

- For optimizing adhesion, the sensitivity to buckling of the structure should be minimized. This allows higher compressive preloads resulting in higher adhesive strength. As hierarchical structures may have a higher propensity for buckling, highly hierarchical structures may not always be beneficial.

- In our study, no benefits were found for the introduction of a third hierarchy level. If adhesion has to be generated against a smooth substrate, a hierarchical system will not result in better results,

27

but may decrease the structure stability and the permissible structure packing density. Also for small roughness amplitudes, a single hierarchical level may still be sufficient.

- The lateral dimensions of the structures have to be much smaller than the wavelength of the substrate. In our studies, we found similar adhesion for hierarchical and non-hierarchical structures with a substrate wavelength 10 times as large as the smallest pillar diameter.

- The effect of microroughness was reasonably well explained by the model of Fuller and Tabor.

- If a high compliance of the structure is necessary, e.g. to accommodate high roughness of the substrate surface, the introduction of hierarchy can lead to a compliance increase by decreasing the buckling load. By buckling "into" asperities, such a structure has the potential of increasing the contact area and hence adhesion.

Although our study on hierarchical surface patterns gave a detailed insight into deformation behaviour and adhesion of more complex geometry, it has to be considered that vertical structures may not be the optimum design for application of bioinspired adhesives due to buckling effects. Future work should therefore consider angled hierarchical structures and their adhesive performance on rough surfaces.

Appendices

Dependence of pull-off force *F* on applied preload P of HL1, HL2 and HL3 with and without mushroom on a flat substrate and photographs of adhesion measurements of a HL2 sample at different positions of a wavy substrate. In addition further force/displacement curves of single size 1 pillars and of seven pillars in a hexagonal array and detailed theoretical estimation of the buckling load for a hierarchical pair of pillars. This material is available free of charge via the Internet at http://pubs.acs.org.

References

[1] Arzt E, Gorb S and Spolenak R 2003 From micro to nano contacts in biological attachment devices *PNAS* **100** 10603–10606

[2] Dirks J-H and Federle W 2011 Fluid-based adhesion in insects – principles and challenges *Soft Matter* **7** 11047–11053

[3] Fratzl P and Barth F G 2009 Biomaterial systems for mechanosensing and actuation *Nature* **462** 442–448

[4] Gao H and Yao H 2004 Shape insensitive optimal adhesion of nanoscale fibrillar structures *PNAS* **101** 7851–7856

[5] Gorb S N, Sinha M, Peressadko A, Daltorio K A and Quinn, R. D. 2007 Insects did it first: micropatterned adhesive tape for robotic applications *Bioinspiration Biomimetics* **2** 117–125

[6] Varenberg M, Pugno N M and Gorb S N 2010 Spatulate structures in biological fibrillar adhesion *Soft Matter* **6** 3269–3272

[7] Autumn K 2006, How Gecko Toes Stick. *American Scientist* **94** 124–132

[8] Berengueres J, Saito S and Tadakuma K 2007 Structural properties of a scaled gecko foot-hair *Bioinspiration Biomimetics* **2** 1–8

[9] Gao H, Wang X, Yao H, Gorb S and Arzt E 2005 Mechanics of hierarchical adhesion structures of geckos *Mech. Mater.* **37** 275–285

[10] Jeong H E and Suh K Y 2009 Nanohairs and nanotubes: Efficient structural elements for gecko-inspired artificial dry adhesives *Nano Today* **4** 335–346

[11] Huber G, Gorb S, Hosoda N, Spolenak R and Arzt E 2007 Influence of surface roughness on

gecko adhesion *Acta Biomater.* **3** 607–610

[12]   Irschick D J, Herrel A and Vanhooydonck B 2006 Whole-organism studies of adhesion in pad-bearing lizards: creative evolutionary solutions to functional problems *J. Comp. Physiol.* **192** 1169–1177

[13]   Pugno N M and Lepore E 2008 Observation of optimal gecko's adhesion on nanorough surfaces *BioSystems* **94** 218–222

[14]   Russell A P and Johnson M K 2007 Real-world challenges to, and capabilities of, the gekkotan adhesive system: contrasting the rough and the smooth *Can. J. Zool.* **85** 1228–1238

[15]   Davies J, Haq S, Hawke T and Sargent J P 2009 A practical approach to the development of a synthetic Gecko tape *Int. J. Adhes. Adhes.* **29** 380–390

[16]   del Campo A, Greiner C and Arzt E 2007 Contact shape controls adhesion of bioinspired fibrillar surfaces *Langmuir* **23** 10235–10243

[17]   Geim A K, Dubonos S V, Grigorieva I V, Novoselov K S, Zhukov A A and Shapoval S Yu 2003 Microfabricated adhesive mimicking gecko foot-hair *Nat. Mater.* **2** 461–463

[18]   Glassmaker N J, Jagota A, Hui C Y and Kim J 2004 Design of biomimetic fibrillar interfaces: 1. Making contact *J. R. Soc., Interface* **1** 23–33

[19]   Gorb S, Varenberg M, Peressadko A and Tuma J 2007 Biomimetic mushroom-shaped fibrillar adhesive microstructure *J. R. Soc, Interface* **4** 271-275

[20]   Greiner C, del Campo A and Arzt E 2007 Adhesion of bioinspired micropatterned surfaces: effects of pillar radius, aspect ratio, and preload *Langmuir* **23** 3495-3502

[21]   Kamperman M, Kroner E, del Campo A 2010 McMeeking, R. and Arzt, E. Functional adhesive surfaces with ''gecko'' effect: the concept of contact splitting *Adv. Eng. Mater.* **12** (5) 335-348

[22]   Murphy M P, Aksak B and Sitti M 2009 Gecko-inspired directional and controllable adhesion S*mall* **5** 170–175

[23]   Paretkar D, Schneider A, Kroner E and Arzt E 2011 In situ observation of contact mechanisms in bioinspired adhesives at high magnification *MRS Commun.* **1** 53-56

[24] Sameoto D and Menon C 2010 Recent advances in the fabrication and adhesion testing of biomimetic dry adhesives *Smart Mater. Struct.* **19** 1–18

[25] Greiner C, Arzt E and del Campo A 2009 Hierarchical gecko-Like adhesives *Adv. Mater.* **21** 479–482

[26] Jeong H E, Lee J-K, Kim H N, Moon S H and Suh K Y 2009 A nontransferring dry adhesive with hierarchical polymer nanohairs *PNAS* **106** 5639–5644

[27] Jeong H E, Lee S H, Kim P and Suh K Y 2006 Stretched polymer nanohairs by nanodrawing *Nano Letters* **6** 1508–1513

[28] Lee H and Bhushan B 2012 Fabrication and characterization of hierarchical nanostructured smart adhesion surfaces *J. Colloid Interface Sci.* **372** 231–238

[29] Lee D Y, Lee D H, Lee S G and Cho K 2012 Hierarchical gecko-inspired nanohairs with a high aspect ratio induced by nanoyielding *Soft Matter* **8** 4905–4910

[30] Liu S Y, Zhang P, Lü H, Zhang C W and Xia Q 2012 Fabrication of high aspect ratio microfiber arrays that mimic gecko foot hairs *Chin. Sci. Bull.* **57** 404–408

[31] Murphy M P, Kim S and Sitti M 2009 Enhanced adhesion by gecko-inspired hierarchical fibrillar adhesives *ACS Appl. Mater. Interfaces* **1** 849–855

[32] Northen M T, Greiner C, Arzt E and Turner K L 2008 A gecko-inspired reversible adhesive *Adv. Mater.* **20** 3905–3909

[33] Yu J, Chary S, Das S, Tamelier J, Pesika N S, Turner K L and Israelachvili J N 2011 Gecko-inspired dry adhesive for robotic applications *Adv. Funct. Mater.* **21** 3010–3018

[34] Yurdumakan B, Raravikar N R, Ajayan P M and Dhinojwala A 2005 Synthetic gecko foot-hairs from multiwalled carbon nanotubes *Chem. Commun.* **30** 3799–3801

[35] Canas N, Kamperman M, Völker B, Kroner E, McMeeking R M and Arzt E 2012 Effect of nano- and micro-roughness on adhesion of bioinspired micropatterned surfaces *Acta Biomater.* **8** 282–288

[36] Pugno N P 2008 Spiderman gloves *Nano Today* **3** 35–41

[37] Yu J, Chary S, Das S, Tamelier J, Turner K L, Israelachvili J N 2012 Friction and adhesion of gecko-inspired PDMS flaps on rough surfaces *Langmuir* **28** 11527-11534

[38] Das S, Cadirov N, Chary S, Kaufman Y, Hogan J, Turner K L and Israelachvili J N 2015 *J. R. Soc., Interface* **12** 20141346

[39] Asbeck A, Dastoor S, Parness A, Fullerton L, Esparza N, Soto D, Heyneman B, Cutkosky M 2009 Climbing rough vertical surfaces with hierarchical directional adhesion *IEEE International Conference on Robotics and Automation* 2675-2680

[40] Lee J, Bush B, Maboudian R, Fearing R S 2009 Gecko-inspired combined lamellar and nanofibrillar array for adhesion on nonplanar surface *Langmuir* **25** 12449-12453

[41] Aksak B, Murphy M P, Sitti M 2008 Gecko inspired micro-fibrillar adhesives for wall climbing robots on micro/nanoscale rough surfaces *IEEE International Conference on Robotics and Automation* 3058-3063

[42] Ruffatto D, Beganovic D, Parness A, Spenko M 2014 Experimental evaluation of adhesive technologies for robotic grippers on micro-rough surfaces *IEEE International Conference on Robotics and Automation* 6150-6155

[43] Ruffato D, Beganovic D, Parness A, Spenko M 2014 Experimental results of a controllable electrostatic/gecko-like adhesive on space materials *IEEE International Conference on Robotics and Automation* 1-7

[44] Li Y, Sameoto D, Menon C 2010 Enhanced compliant adhesive design and fabrication with dual-level hierarchical structure *Journal of Bionic Engineering* **7** 228-234

[45] Krahn J, Sameoto D, Menon C 2011 Controllable biomimetic adhesion using embedded phase change material *Smart Mater. Struct.* **20** 1-8

[46] Gillies A G, Henry A, Lin H, Ren A, Shiuan K, Fearing R S and Full R J 2014 Gecko toe and lamellar shear adhesion on macroscopic, engineered rough surfaces *The Journal of Experimental Biology* **217** 283-289

[47] Gillies A G, Fearing R S 2014 Simulation of synthetic gecko arrays shearing on rough surfaces *J. R. Soc., Interface* **11** 20140021

[48] Bhushan B, Peressadko A G and Kim T-W 2006 Adhesion analysis of two-level hierarchical morphology in natural attachment systems for 'smart adhesion' *J. Exp. Biol.* **20** 1475– 1491

[49] Kim T W and Bhushan B 2007 Adhesion analysis of multi-level hierarchical attachment system contacting with a rough surface J. *Adhesion Sci. Technol.* **21** 1–20

[50] Sauer R A 2009 A three-dimensional multiscale finite element model describing the adhesion of a gecko seta *Proc. Appl. Math. Mech.* **9** 157-158

[51] Kroner E and Arzt E 2012 Single macropillars as model systems for tilt angle dependent adhesion measurements *Int. J. Adhes. Adhes.* **36** 32-38

[52] Kroner E and Arzt E 2013 Mechanistic analysis of force–displacement measurements on macroscopic single adhesive pillars *J. Mech. Phys. Solids* **61** 1295-1304

[53] Lakhera N, Graucob A, Schneider A S, Kroner E, Arzt E, Yakacki C M and Frick C P 2013 Effect of viscoelasticity on the spherical and flat adhesion characteristics of photopolymerizable acrylate polymer networks *Int. J. Adhes. Adhes.* **44** 184-194

[54] Lakhera N, Graucob A, Schneider A S, Kroner E, Micciche M, Arzt E and Frick C 2013 Adhesion behavior of polymer networks with tailored mechanical properties using spherical and flat contacts *MRS Commun.* **3** 73-77

[55] Micciché M, Arzt E and Kroner E 2014 Single Macroscopic Pillars as Model System For Bioinspired Adhesives: Influence of Tip Dimension, Aspect Ratio, and Tilt Angle *ACS Appl. Mater. Interfaces* **6** 7076-7083

[56] Kroner E, Blau J and Arzt E 2012 Note: An adhesion measurement setup for bioinspired fibrillar surfaces using flat probes *Rev. Sci. Instrum.* **83** 016101

[57] Kroner E, Maboudian R and Arzt E 2010 Adhesion Characteristics of PDMS Surfaces During Repeated Pull-Off Force Measurements *Adv. Eng. Mater.* **12** 398-404

[58] Kroner E, Paretkar D, McMeeking R and Arzt E 2011 Adhesion of Flat and Structured PDMS Samples to Spherical and Flat Probes: A Comparative Study *J. Adhes.* **87** 447-46

[59] Biot M A 1963 Exact theory of buckling of a thick slab *Appl. Sci. Res.* A **12** 183-198

[60] Heepe L, Carbone G, Pierro E, Kovalev A E Gorb S N 2014 Adhesion tilt-tolerance in bio-inspired mushroom-shaped adhesive microstructure *Appl. Phys. Lett.* **104** 011906 1-5

[61] Aksak B, Sahin K, Sitti M 2014 The optimal shape of elastomer mushroom-like fibers for high and robust adhesion *Beilstein J. Nanotechnology* **5** 630-638

[62] Paretkar D, Kampermann M, Schneider A S, Martina D, Creton C and Arzt E 2011 Bioinspired pressure actuated adhesive system *Mater. Sci. Eng. C* **31** 1152–1159

[63] Paretkar D, Kamperman M, Martina D, Zhao J, Creton C, Lindner A, Jagota A, McMeeking R and Arzt E 2013 Preload-responsive adhesion: effects of aspect ratio, tip shape and alignment *J. R. Soc., Interface* **10** 73-77

[64] Fuller K N G and Tabor D 1975 The Effect of Surface Roughness on the Adhesion of Elastic Solids *Proc. R. Soc. Lond.* A **345** 327-342

Hierarchical macroscopic fibrillar adhesives: In-situ study of buckling and adhesion mechanisms on wavy substrates

Christina T. Bauer[1,3], Elmar Kroner[1], Norman A. Fleck[2], Eduard Arzt[1,3]

[1]INM – Leibniz Institute for New Materials, Campus D2 2, 66123 Saarbrücken, Germany

[2]University of Cambridge, Engineering Department, Trumpington Street, Cambridge, CB2 1PZ, UK

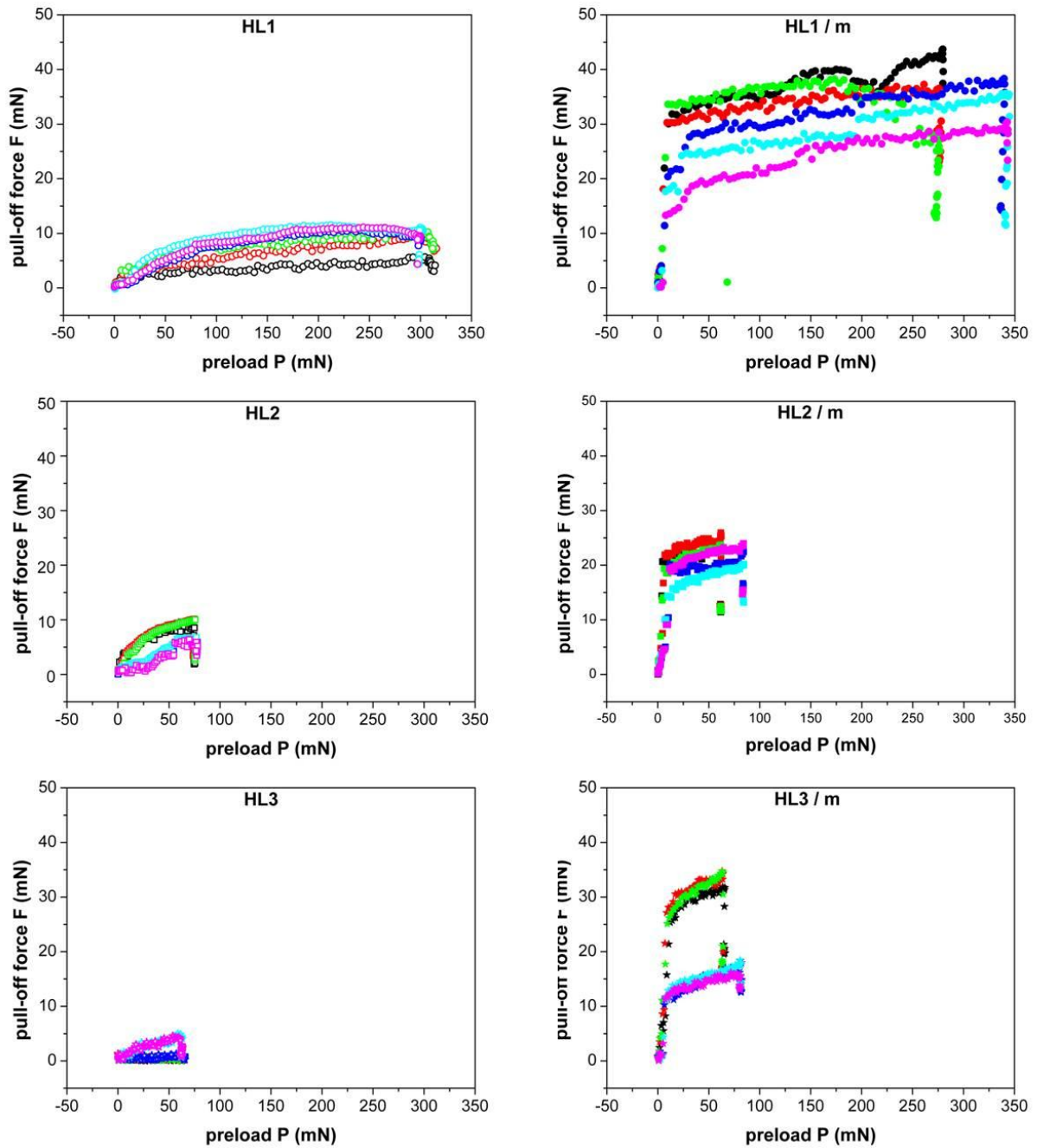[3]Saarland University, Campus D2 2, 66123 Saarbrücken, Germany

E-mail: eduard.arzt@leibniz-inm.de

Appendices

Figure A1: Dependence of pull-off force F on applied preload P of HL1, HL2 and HL3 with (/ m) and without mushrooms on a flat probe.
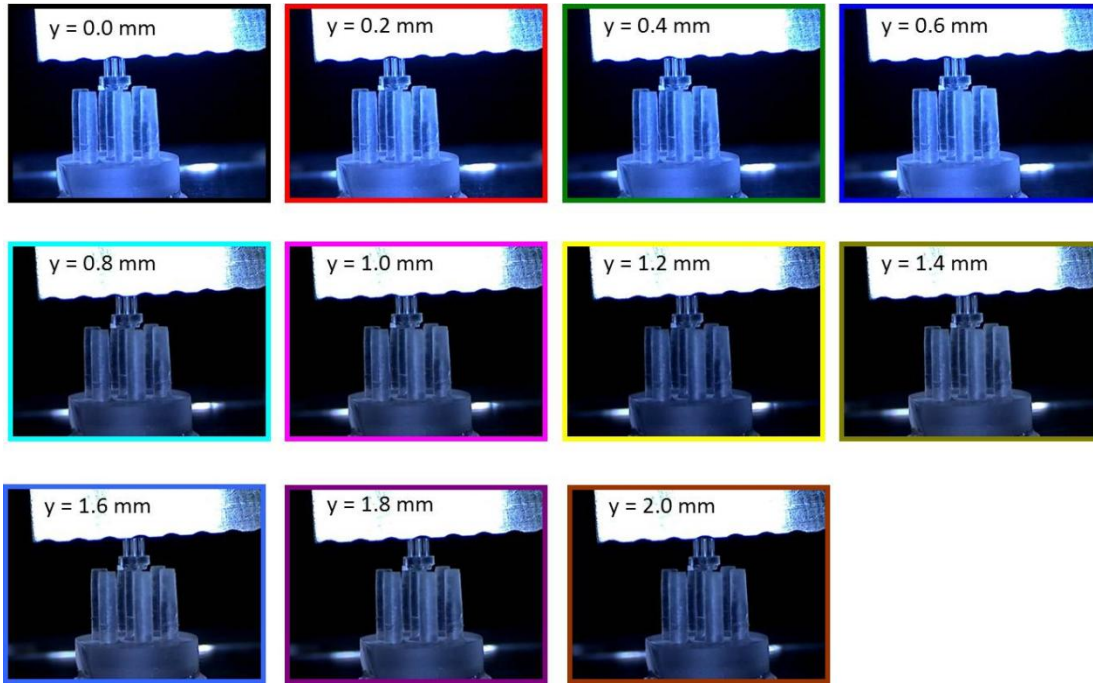
Figure A2: Adhesion measurements of a HL2 sample at different positions of a wavy substrate. For each measurement, the sample was shifted by 0.2 mm.
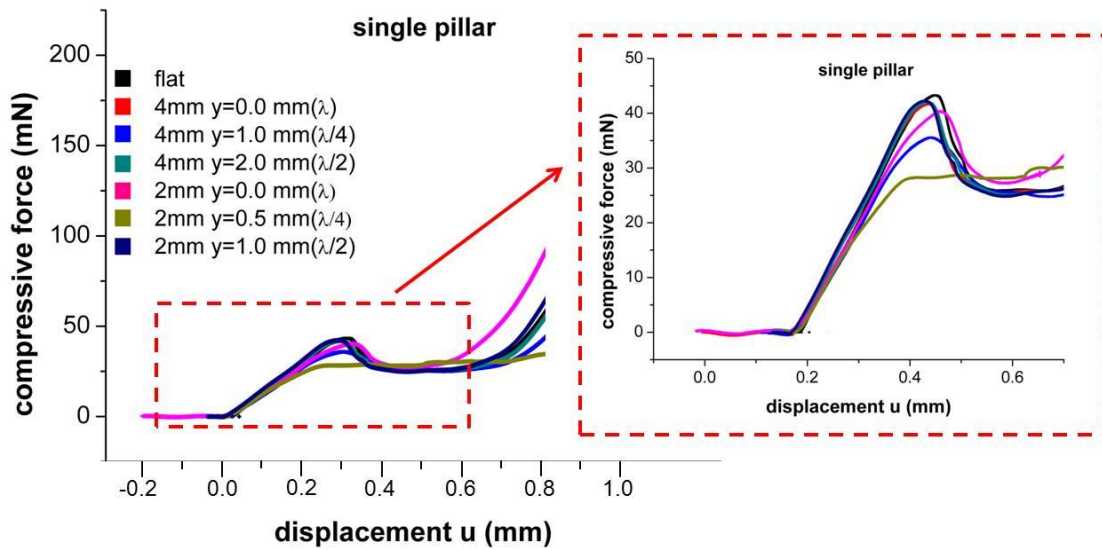

Figure A3: Force/displacement curves measured on a flat, on a truncated wavy probe (λ = 2 mm, h = 200 µm) and on wavy probe (λ = 4 mm, h = 200 µm). The results of the measurement curves are based on size 1 single pillar (sp) measurement results.
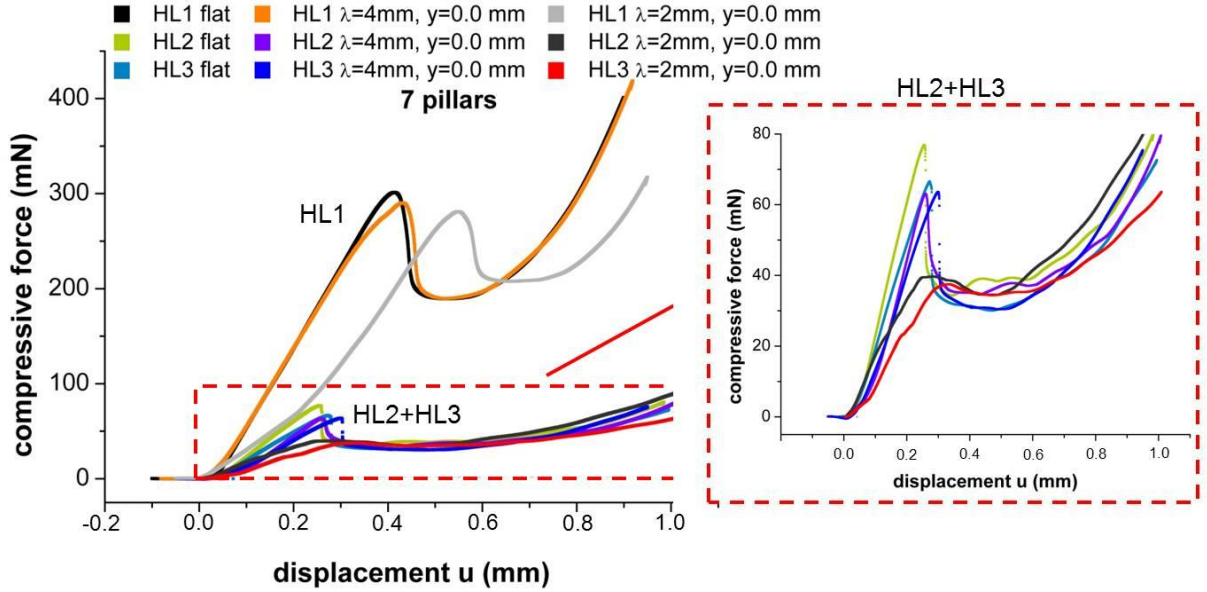
Figure A4: Force/displacement curves measured on a flat, on a truncated wavy probe ($\lambda = 2$ mm, h = 200 µm) and on wavy probe ($\lambda = 4$ mm, h = 200 µm). The results of the measurement curves are based on a HL1, HL2 and HL3 hexagonal pillar assembly (hp).

A1. Detailed estimation of the buckling load for a hierarchical pair of pillars

Consider the elastic buckling response of a pillar which has a stepwise jump in bending modulus along its length. The top pillar 1, of length ℓ_1 and bending modulus $(EI)_1$, is supported by an underlying pillar 2, of length ℓ_2 and bending modulus $(EI)_2$, as shown in Figure A5. The top end of pillar 1 is subjected to an end load P and is restrained against lateral motion by a force F, which only develops in the buckled state. The top end of beam 2 is adhered to the bottom of pillar 1, while the bottom end of pillar 2 is fully clamped. Now consider the buckled state of pillars 1 and 2. In the buckled state, the pillars deflect transversely into the shape $u(x)$. At any section x, the bending moment distribution is $M = (EI)_i\, u''(x)$ (for columns i=1, 2), where the prime denotes differentiation with respect to x, and

38

$$M(x) = (EI)_i u''(x) = Fx - Pu \tag{A.1}$$

This second order differential equation has solution

$$u(x) = A \sin \omega_1 x + \frac{F}{P}x \tag{A.2}$$

for pillar 1 and

$$u(x) = B \sin \omega_2 x + C \cos \omega_2 x + \frac{F}{P}x \tag{A.3}$$

for pillar 2, where

$$\omega_i{}^2 = \frac{P}{(EI)_i} \qquad \text{for i=1,2} \tag{A.4}$$

Imposition of the end conditions $u(l_1 + l_2) = u'(l_1 + l_2) = 0$ gives

$$C = -B \frac{(\sin\xi - \xi\cos\xi)}{(\cos\xi + \xi\sin\xi)} \tag{A.5}$$

where $\xi = (\ell_1 + \ell_2)\omega_2$. Now impose continuity of $u(l_1)$ and $u'(l_1)$ at the junction between pillars 1 and 2. Then, (A.2) and (A.3), along with (A.5), imply

$$\begin{pmatrix} a_{11} & a_{12} \\ a_{21} & a_{22} \end{pmatrix} \begin{pmatrix} A \\ B \end{pmatrix} = \begin{pmatrix} 0 \\ 0 \end{pmatrix} \tag{A.6}$$

where

$$a_{11} = (\cos\xi + \xi\sin\xi)\sin\omega_1 l_1 \tag{A.7a}$$
$$a_{12} = (\sin\xi - \xi\cos\xi)\cos\omega_2 l_1 - (\cos\xi + \xi\sin\xi)\sin\omega_2 l_1 \tag{A.7b}$$
$$a_{21} = (\cos\xi + \xi\sin\xi)\omega_1 l_1 \cos\omega_1 l_1 \tag{A.7c}$$
$$a_{22} = -(\sin\xi - \xi\cos\xi)\omega_2 l_1 \sin\omega_2 l_1 - (\cos\xi + \xi\sin\xi)\omega_2 l_1 \cos\omega_2 l_1 \tag{A.7d}$$

Finite values for (A, B) are obtained when the determinant of a_{ij} vanishes, thereby defining the buckling equation for the load P. It is convenient to non-dimensionalise the problem to the form

$$\frac{P}{P_E} = f\left(\frac{(EI)_1}{(EI)_2}, \frac{l_2}{l_1}\right)$$

where $P_E = \pi^2 (EI)_1/{l_1}^2$ is the Euler buckling load for a pillar of length l_1, and bending modulus $(EI)_1$, and pivoted at both ends. Contours of P/P_E are plotted as a function of $\frac{(EI)_1}{(EI)_2}$ and $\frac{l_2}{l_1}$ in Figure A6 by solving for det $(a_{ij}) = 0$ using a root finding algorithm within MATLAB.
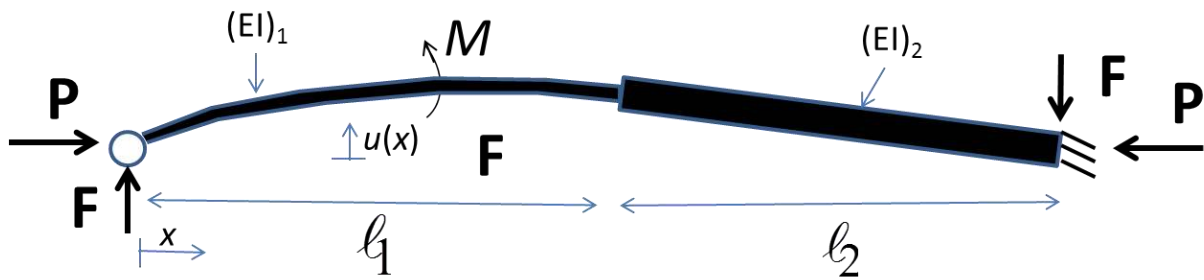

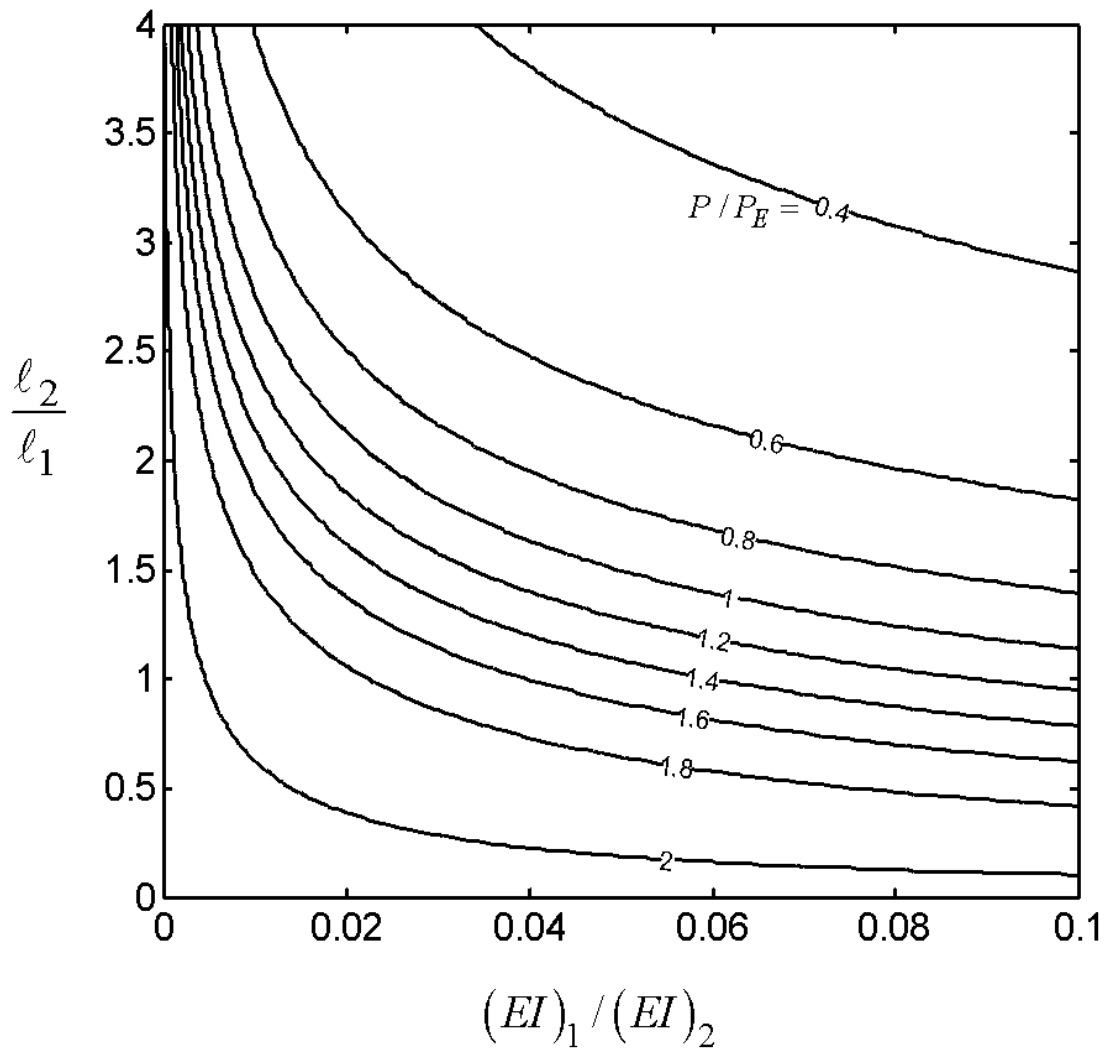Figure A5: Schematic of the buckling/bending process of a HL2 with parameters.

Figure A6: Contours of P/P_E

$P/P_E = 0.423$. For a single pillar (size 1), $P/P_E = 2.05$, and so the ratio of buckling strength for HL1 and HL2 is $2.05/0.423 = 4.8$.